Journal of Materials Chemistry A



PAPER View Article Online
View Journal | View Issue



Cite this: J. Mater. Chem. A, 2023, 11, 2814

Received 17th November 2022 Accepted 25th December 2022

DOI: 10.1039/d2ta08988b

rsc.li/materials-a

A metal-free all-organic ammonium-ion battery with low-temperature applications†

Shelton Farai Kuchena and Ying Wang **

Current commercial batteries are mainly metal based, with metal elements in charge carriers and/or electrode materials, which poses potential economic and environmental concerns due to the heavy use of nonrenewable metals. Thus, metal-free batteries present a unique opportunity as sustainable energy storage devices, though the relevant research is still in its infancy. Herein, we present an all-organic metal-free NH₄⁺ ion full battery that can operate at a low temperature of 0 °C, by using polypyrrole (PPy) as the cathode, polyaniline (PANI) as the anode, and 19 m ammonium acetate aqueous solution as electrolyte. For the first time, PPy is demonstrated as a high-capacity host material for both NH_4^+ and K^+ storage, when cycled in water in salt electrolytes (WiSEs). When tested in a three-electrode cell containing 25 m NH_4CH_3COO electrolyte, PPy exhibits an impressive capacity of 125 mA h g^{-1} at a specific current of 1 A q^{-1} and retains 43.61 mA h q^{-1} at 25 A q^{-1} . Additionally, a full battery is assembled using the PPy cathode and PANI anode coupled with 19 m NH₄CH₃COO WiSE. This battery is found to deliver a capacity of 78.405 mA h $\rm g^{-1}$ at 25 °C and 49.083 mA h $\rm g^{-1}$ at 0 °C with a capacity retention of 71.83% after 200 cycles, demonstrating its potential for operations at low temperatures. Additionally, the physiochemical properties of $\mathrm{NH_4}^+$ -based WiSEs are examined by Raman and nuclear magnetic resonance (NMR) spectroscopies, to explore their electrochemical behaviors and the fundamental effect of salt concentration on the electrolyte characteristics. This study presents the first non-metal battery with potential for low-temperature applications and opens the door to future metalfree electronics that would generate long-term benefits to the environment.

Introduction

To realize the full potential of renewable energy technology, a system such as a battery that can store the harvested energy efficiently plays a pivotal role. Additionally, the fast-advancing technological gadgets, electric vehicles and smart grids all require energy storage devices, e.g., batteries, to power them. Lithium-ion batteries (LIBs) that rely on inorganic electrodes (e.g., LiCoO₂, 1,2 LiFePO₄ (ref. 3) and LiMnO₂ (ref. 4)) currently dominate the market as inexpensive mobile energy storage devices delivering high energy density. 5,6 Nevertheless, the price of LIBs has been steadily increasing over the past years, due to the scarcity of Li and Co, which hinders their application in large grid-scale energy storage.7 In addition, LIBs usually employ organic electrolytes that are flammable/toxic and thus pose significant safety concerns. Therefore, there has been intense interest in studying alternative metallic charge carriers in batteries, such as Na⁺ and K⁺, as well as multivalent metallic ions including Al³⁺, Zn²⁺, Mg²⁺, etc.⁸⁻¹² However, batteries based

Department of Mechanical & Industrial Engineering, Louisiana State University, Baton Rouge, LA 70803, USA. E-mail: ywang@lsu.edu on these metallic charge carriers are limited by high electrostatic attraction or repulsion between the multivalent ions and electrode, electrode corrosion by electrolyte, active material dissolution, self-aggregation and phase change during (de) intercalation.

To address the challenges above, researchers have recently shifted their attention to nonmetal charge carriers in electrochemical energy systems, such as the proton (H⁺), hydronium (H_3O^+) , and ammonium (NH_4^+) . Among the three, the NH_4^+ ion is the most appealing, because NH₄⁺ electrolyte presents a mildly acidic environment, whereas H⁺ or H₃O⁺ electrolyte has a lower pH, causing corrosion of electrodes. NH₄⁺ ions offer many preferable characteristics compared to metallic charge carriers such as they are sustainable and are nontoxic regarding their disposal. When it comes to manufacturing the NH₄⁺ ion can be produced from nitrogen and hydrogen which are abundant in air. It also has a very low molar mass of 18 mol g⁻¹ which is beneficial for the development of high-energy-density batteries. Additionally, it has the smallest hydration radius of 3.31 Å despite a large ionic radius of 1.48 Å, resulting in faster kinetics in the electrolyte. ¹³ Finally, the NH₄ ion entails flexible hydrogen bonds with host materials, which are different and weaker than the ionic bonds between metallic charge carriers and electrodes. Nevertheless, the large ionic radius of the

[†] Electronic supplementary information (ESI) available. See DOI: https://doi.org/10.1039/d2ta08988b

ammonium ion requires host materials with larger open structures to accommodate it during charging/discharging, which limits the electrode material choices. The large ionic size also affects the desolvation process of ammonium ions, causing sluggish redox kinetics, increased polarization of a full $\mathrm{NH_4}^+$ ion battery (AIB) and consequent inferior electrochemical performance.

A variety of electrode materials have been reported for storing NH₄⁺ ions, as described below. The pioneering work in NH₄⁺ ion batteries was performed by Yi Cui's group using Prussian blue analogues, i.e., NiHCF and CuHCF mainly because of their open structure and strong structural integrity, delivering a capacity of 55 mA h g⁻¹ and 51.3 mA h g⁻¹, respectively. 14,15 Various PBAs have been used as cathode materials for NH₄⁺ ion storage, such as MnHCF, ¹⁶ Berlin green, Fe₄[Fe(CN)₆]₃, K_{0.9} Cu_{1.3}Fe(CN)₆, V_{1.5}Fe(CN)₆, CN $NaFe^{III}[Fe^{II}(CN)_{6}]$, ²¹ $Na_{1.45}Fe[Fe(CN)_{6}]_{0.93}$ (ref. 22) and $(NH_{4})_{2}Cu$ [Fe(CN)₆].²³ Additionally, transition metal oxides have been used as cathode materials in different battery systems because of their layered structure. MoO₃,²⁴ V₂O₅,²⁵ Fe₅V₁₅O₃₉(OH)₉- $\cdot 9H_2O$, 26 NH $_4V_3O_8$, 27 and MnO, 28 have been found to be promising NH₄⁺ ion storage materials, exhibiting a capacity of 120, 70, 130, 120 and 175 mA h g^{-1} , respectively. Since diluted aqueous electrolyte restricts the voltage window as narrow as 1.23 V due to the hydrogen/oxygen evolution, "water-in-salt" electrolyte (WiSE) has been used by dissolving highconcentration salts in water, as pH increases with the salt concentration and hydrolysis is reduced.²⁹ As such, the Ji group employed 25 m ammonium acetate solution as WiSE to be combined with the naphthalenetetracarboxylic dianhydridederived polyimide (PNTCDA) electrode, leading to a battery showing a wider potential window of 2.95 V.30 Moreover, hydrogel electrolytes have been used to fabricate quasi-solidstate flexible $\mathrm{NH_4}^+$ ion batteries. For instance our group designed a flexible NH4+ ion battery based on a hydrogel electrolyte synthesized using Xanthan gum, exhibiting a capacity of 55 mA h g⁻¹ and excellent mechanical properties when bent at different angles.26 Though progress has been made in the area of AIBs, their capacities are still limited compared to their metallic charge carrier counterparts.

Batteries manufactured from metallic elements such as Ni, Co, and Li, have been termed the new "petroleum" due to the imminent scarcity of these metallic elements. The dependence on metallic elements also causes environmental concerns due to toxicity of some metals and lack of sustainability.31 On the other hand, non-metal charge carriers make it possible to fabricate safer and more sustainable metal-free batteries by combining with organic electrodes. Compared to traditional inorganic electrodes, organic electrodes have recently attracted much attention owing to their tunable molecular structure, metal-free feature, and lightness. They can be particularly useful for AIBs, because their flexible molecular structure could accommodate the large ionic size of ammonium ions. Redoxactive organic materials (ROMs), with organic groups from C, O, N and S have emerged as electroactive materials due to their abundance and light weight. They can be classified into three different categories depending on their charge storage

mechanisms, *i.e.*, p, n, and bipolar. $^{32-35}$ A p-type ROM has a charge storage mechanism in which oxidation occurs in the positively charged state (P^+), losing an electron, and the charge will then be balanced by an anion. An n-type ROM (N) gets reduced by accepting an electron resulting in the negatively charged group and a counter positive cation balances this charge. In a bipolar type, a combination of both storage mechanisms of p and n types occurs.

Recently, a metal-free NH₄⁺ dual-ion battery has been reported by using a graphite cathode and a 3,4,9,10-perylenetetracarboxylic anode, which exhibits an energy density of 200 W h kg⁻¹ when cycled in an organic electrolyte with NH₄PF₆ dissolved in the hybrid solvents of adiponitrile and ethyl methyl carbonate.36 Though a potential high voltage of 2.75 V is shown in this proof-of-concept work, the battery is cycled in a much narrower potential range and exhibits moderate capacities. Additionally, both the electrode and the electrolyte materials used in this work are quite expensive. Among various organic electrodes, polypyrrole (PPy) and polyaniline (PANI) have been used as electrodes in metal ion batteries,37-40 as they can be oxidized with anions through doping increasing their electrical conductivity. Polarons and bipolarons formed on the conjugated backbones upon p-type doping process, increase their energy levels and conductivity. Both these polymers offer advantages of facile synthesis. Our group made the first effort to demonstrate PANI as a promising host material for NH₄⁺ ion storage, recording a capacity of 160 mA h g⁻¹ at 1 A g⁻¹.41 We also prepared V₂O₅ intercalated with PANI for NH₄⁺ ion storage, which delivers an increased capacity of 195.5 mA h g⁻¹ at 1 A g⁻¹. 42,43 Nevertheless, PPy has never been tested for ammoniumion storage so far.

In this work, a metal-free ammonium-ion battery is developed using PPy and PANI electrodes coupled with WiSE. PPy is tested as a host material for NH₄⁺ and K⁺ ions, as they have similar physical properties, i.e., the same coordination number (CN) of 6, and an ionic radius of 1.38 Å for K⁺ vs. an ionic radius of 1.48 Å. Additionally, water in salt electrolyte (WiSE) is employed to improve the performance of the batteries, as WiSE offers better properties than conventional electrolytes, including expanded electrochemical window, inhibited parasitic side reactions, and suppressed metal dissolution. Another advantage provided by WiSE is a lower freezing point due to fewer free water molecules in WiSE compared to conventional diluted electrolytes, which makes it possible to develop batteries that can operate at subzero temperatures. Herein, we investigate K⁺/NH₄⁺ ion insertion in ROM PPy using 25 M and 1 M electrolytes of KAc or NH₄Ac. Additionally, this work is the first effort to fabricate a nonmetal full battery that can operate at a low temperature of 0 °C, by using a ROM PPy cathode, PANI anode, and 19 m NH₄Ac electrolyte.

Results and discussion

PPy was prepared via a chemical oxidation method using anhydrous FeCl₃ as a chemical oxidant, as described in the Experimental procedure in the ESI.† The yield and conductivity of PPy produced are affected by the solvent, type of oxidant,

Scheme 1 Reactions for synthesizing PPy via chemical oxidation.

monomer/oxidant ratio, and reaction time. The optimum ratio of Fe(III) to the monomer of 2.4 will result in the yield of PPy approaching 100%.⁴⁴ The overall reaction is represented by the following stoichiometric reaction equation:

$$nC_4H_5N + (2 + y)nFeCl_3 = [(C_4H_3N)_n^{y+}nyCl^-] + (2 + y)nFeCl_2 + 2nHCl$$
 (1)

where *y* is the degree of PPY oxidation.

Scheme 1 presents the formation reactions of the PPy polymer. $FeCl_3$ serves as the oxidant which produces active cation-radicals of the monomers while the reaction proceeds, resulting in a long conjugated structure with C=C bonds and C-C

bonds alternately arranged. An optimum ratio of the oxidant to the monomer is required. If the ratio is too high, more oxidant will be available, resulting in overpolymerization. If the ratio is too low, the polymerization would not be completed, and more monomer units will be left in the solution.⁴⁵

The as-prepared PPy is then characterized for composition, structure, and morphology, as revealed in Fig. 1. Fig. 1a shows the SEM image of PPy, displaying a highly porous nano-thorn structure which is beneficial to electrochemical redox reactions as it provides a high surface area and short diffusion paths. Fig. 1b presents the EDS spectrum of PPy, showing its elemental composition with C - 77.8%, O - 9.9%, and N - 9.6%, confirming the successful synthesis of PPy. The EDS mapping in

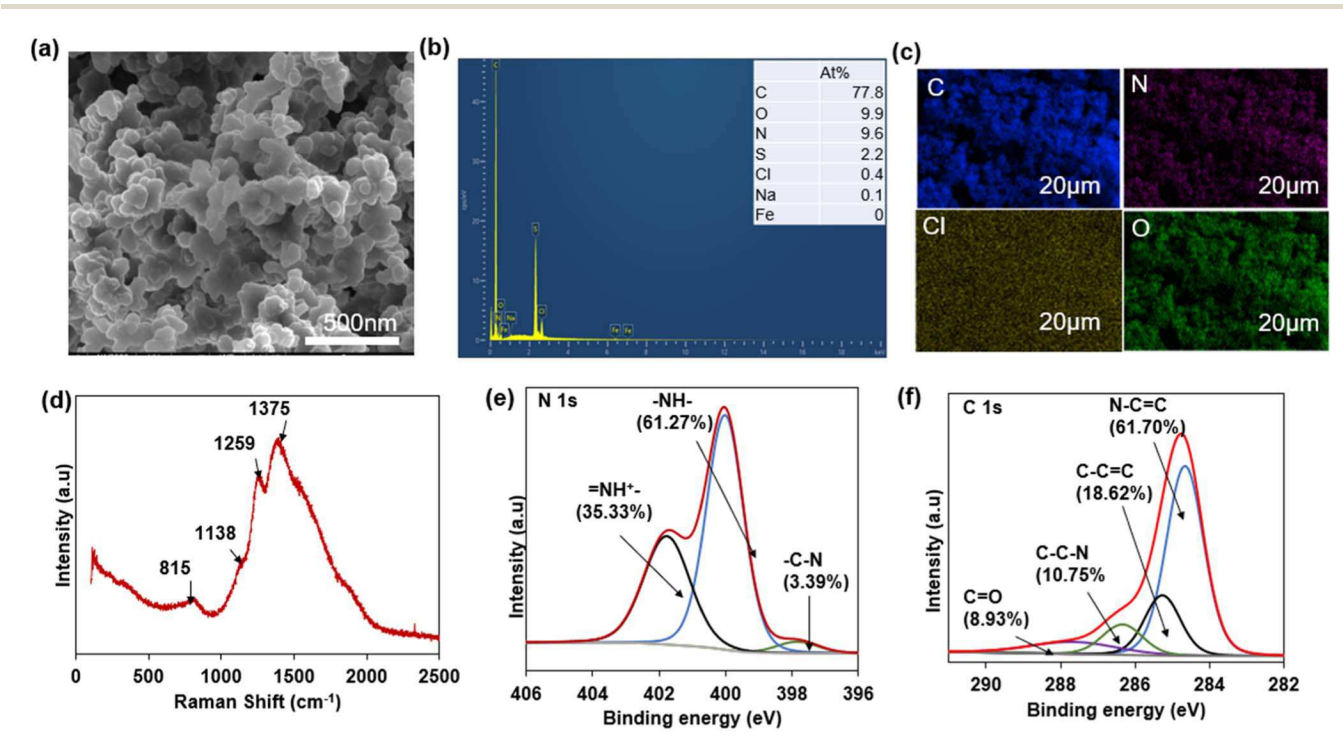


Fig. 1 (a) SEM image, (b) EDS spectrum, (c) EDS mapping, and (d) Raman spectrum, (e) XPS N 1s spectrum, and (f) XPS C 1s spectrum of PPY.

Fig. 1c suggests the homogeneous distribution of C, N, O and Cl in the entire sample, indicating a uniform composition of PPy. Fig. 1d displays the Raman spectrum of PPy, with the bands at 815 and 1138 cm⁻¹ assigned to the ring formation associated with the dication (di-polaron) and the radical cation (polaron), the peak at 1375 cm⁻¹ attributed to the C-N stretching mode and that at 1259 cm⁻¹ is the C-H group, again demonstrating the successful synthesis of PPY.46 Fig. 1e displays the N 1s XPS spectrum of PPy that shows nitrogen groups at 400.03, 401.77 and 397.75 eV corresponding to -NH- with an atomic weight percentage of 61.27%, -NH⁺- with 35.33%, and -C-N with 3.39%, respectively.⁴⁷ The presence of FeCl₃ during synthesis would result in polarons and bipolarons that have a delocalized spin which is responsible for the conductivity of PPY. Additionally, Fig. 1f presents the C1s XPS spectrum revealing peaks at 284.5 eV, 285.1, 286.5, and 287.7 eV, representing the N-C= C, C-C-C, N-C-C- and -C=O- groups in PPy. X-ray diffraction (XRD) is performed to examine the crystallinity of PPy powders which are found to be amorphous as shown in Fig. S1.† A broad peak is observed at about $2\theta = 21.89^{\circ}$ which is characteristic of amorphous PPy due to the scattering from PPy chains at the interplanar spacing.48

To explore the physiochemical properties of the electrolytes with various concentrations, we perform linear sweep voltammetry (LSV) as well as Raman and ¹H NMR spectra characterization studies. First, LSV is carried out to determine the potential window of the aqueous ammonium-ion electrolytes,

as presented in Fig. 2a. It is found that the 25 m NH₄Ac electrolyte shows a potential window of 2.722 V, wider than 2.120 V from the 1 m NH₄Ac electrolyte. The expanded voltage window is attributed to the anodic stability properties, though the electrolyte concentration has an insignificant effect on the water cathodic stability. 49,50 In order to understand the interaction between the ammonium acetate salt and water, Raman spectroscopy is performed on the electrolytes with concentrations of NH₄Ac varying from 1 to 25 m as displayed in Fig. 2b. The O-H stretching vibration peaks reveal that the spectrum of WiSE resembles that of the crystalline salt with no water molecules, while a broad Raman band is observed for pure water, due to water molecules in different hydrogen bonding environments in water clusters.51 This band remains pronounced in the electrolyte of 1 m NH₄Ac, indicating that water molecules remain clusters and do not participate that much in the hydration structure around the NH₄⁺ ions. As the salt concentration increases to 25 m, it is observed that a sharp peak progressively forms at 2934.988 cm⁻¹ at the expense of the broad water cluster band, suggesting that the number of free water clusters decreases significantly and the vast majority of water molecules are in a state of crystalline hydrates. 49 These results illustrate that the lower the water content available for the formation of the solvation sheath, the sharper the peak becomes. The position of the peak also depends on the salt, e.g., 3552 cm⁻¹ for 17 m $NaClO_4^{52}$ and 3429 cm⁻¹ for 40 m HCOOK.⁵³

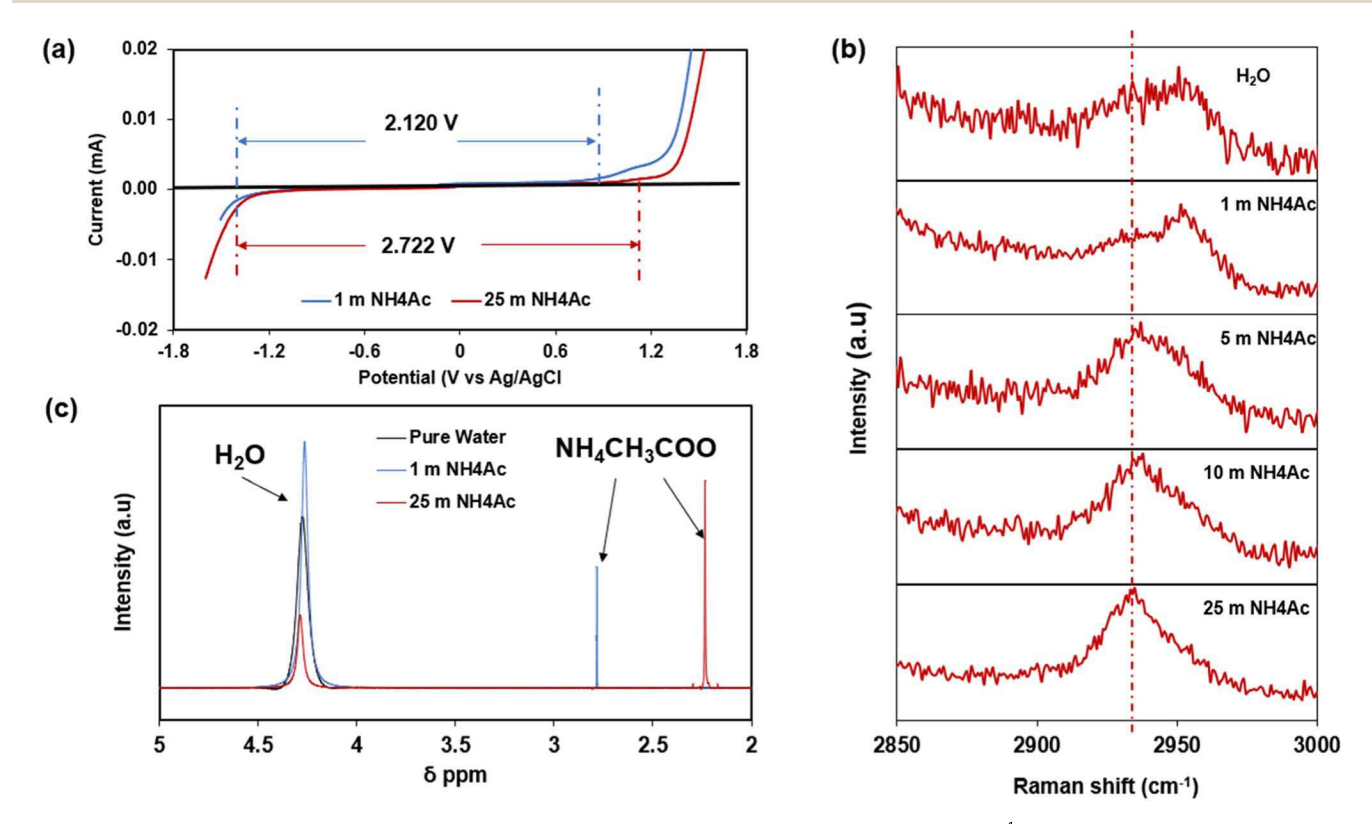


Fig. 2 (a) Linear sweep voltammetry curves recorded in 1 m and 25 m NH_4Ac electrolytes at 10 mV s⁻¹. The onset potentials are selected at 0.001 mA. (b) The Raman bands are observed in the range of 2900 to 3000 cm⁻¹ which correspond to the O–H stretching modes of water. (c) Normalized NMR spectra of 1 m and 25 m NH_4Ac electrolytes as well as pure water, showing the ¹H chemical shift of water molecules and protons in NH_4Ac .

To further explore the interactions between ions and water molecules as well as the hydrogen bonding in the electrolytes, proton NMR studies are performed on the 1 m and 25 m NH₄Ac electrolytes in addition to pure water as a reference, as revealed in Fig. 2c. The downward chemical shift from 2.783 to 2.236 ppm for the ¹H spectra from NH₄CH₃COO is due to the increase in concentration as the interaction between the NH₄Ac ions and water molecules increases.54 The NH4+ ion is multipolar and can form hydrogen bonds in aqueous solution, entailing a redox chemistry different from the ionic bonds formed by metallic charge carriers. The formation of hydrogen bonds is more pronounced at higher concentrations of salt, due to the increase of interaction between the cations and water molecules, leading to the shift in the ¹H NMR spectra. It is noted that the interaction between the NH₄⁺ ion and oxygen in water is much stronger with a larger binding energy of 0.89 eV than that between two water molecules (0.27 eV). In this regard, more hydrogen bonds are formed between NH₄⁺ ions and -OH (in water) in the high-concentration electrolyte containing fewer free water molecules. In high-concentration electrolyte, significant ion-pairing and aggregation occur while a limited number of solvent molecules will be largely bound to cations, leading to new electrolyte structures at both molecular and long-range scales that would affect properties such as transport, thermal, mechanical, electrochemical, interfacial, and interspatial. In a diluted solution, cations exist as hydrated ions bound by water molecules. However, there are more cations than water molecules in the WiSE, hence, the primary solvation sheath of a cation is not complete, resulting in fewer water molecules available for the formation of the primary solvation sheath of the ion. The reduced solvation number decreases the highest occupied molecular orbital (HOMO) level of water, making water splitting reactions more difficult, especially the oxygen evolution reaction (OER). Additionally, fewer free water molecules would cause the suppressed freezing point of the aqueous electrolyte.55

In this work, NH₄⁺ and K⁺ ions are compared as charge carriers for battery performance evaluation, since these two ions have similar physical properties, such as the same coordination number (CN) = 6 and an ionic radius of 1.38 Å for $K^+ \nu s$. 1.48 Å for NH₄⁺. To study the intercalation behaviors of these two ions in the PPy electrode, a three-electrode cell is set up, using PPy as the working electrode, graphite as the counter electrode, and Ag/AgCl as the reference electrode in 1 m or 25 m electrolyte. Fig. 3a-d present the cyclic voltammogram (CV) curves of the battery cells using 25 m and 1 m NH₄Ac and KAc electrolytes, respectively. The CV area from the cell using 25 m NH₄Ac electrolyte in Fig. 3a appears larger than that from the 25-m-KAc-based cell in Fig. 3c, suggesting that PPy delivers higher NH₄⁺-storage capacity than K⁺-storage capacity. Fig. 3a displays the first three CV curves for PPy in 25 M NH₄Ac in a voltage range of -1 V to 0.5 V. The cathodic peaks, located at -0.541, -0.136 and 0.168 V, are observed during the initial reduction scan, which overlap well with the three peaks in the following cycles of the cathodic scan. The oxidation peaks located at -0.303, -0.06 and 0.456 V also overlap well in the first three CV curves. Multiple oxidation-reduction pairs of peaks are clearly

observed, suggesting a multistep reaction process of NH₄⁺ ions with the PPy electrode. Furthermore, the CV profiles of the three initial cycles show good repeatability, indicating good redox reversibility and structural stability of the PPy electrode. These curves are slightly different from those of PPy for K⁺ storage in the 25 M KAc electrolyte in Fig. 3c which reveals cathodic peaks at -0.023 and -0.5 V as well as oxidation peaks at 0.227 and −0.272 V. The CV profiles of PPy for K⁺ storage also show good repeatability, suggesting good reversibility. The CVs for K⁺ and NH₄⁺ storage in PPy display clear redox peak pairs, demonstrating the capability of PPy in stable and reversible electrochemical storage of both K⁺ and NH₄⁺ ions. In contrast, the CV for NH₄⁺ intercalation shows an additional redox peak pair compared to that for K⁺ intercalation, attributed to a different multistep reaction process. The NH₄⁺ ion exhibits a structure composed of four flexible hydrogen atoms which make it multipolar and can form hydrogen bonds with the host structure. Hence, the NH₄⁺ ion entails a different redox chemistry from the metallic K⁺ ion that forms a rigid ionic bond with the host. It is important to note that the desolvation process in aqueous electrolyte requires a lower energy for NH₄⁺ ions than that for K⁺ ions, because NH₄⁺ ions form hydrogen bonds with water molecules which are weaker than the ionic bonds formed by K⁺ ions.⁵⁶ Fig. 3b and c show the first three CV curves of the PPy electrode in 1 M aqueous electrolyte with NH₄Ac or KAc, respectively. In 1 m NH₄Ac, the CV of PPy reveals an anodic peak at -0.60 V and a cathodic peak at -0.39 V which have different peak positions than those in the CV from the 1 M KAc electrolyte with anodic peaks at -0.526 and 0.295 V and a cathodic peak at -0.429 V. For both NH₄⁺ and K⁺ storage, the peaks on the CV curves of PPy from the 1 m electrolyte are fewer and less sharp than those from the 25 m electrolyte, due to different intercalation mechanisms in the electrolytes of different concentrations. It is also observed that the CV curves from the 25 m electrolytes exhibit a higher integrated area than that from the 1 m electrolyte, suggesting that the battery cell based on WiSE may deliver higher specific capacity than that using the diluted electrolyte.

It is important to evaluate the rate performance of aqueous ammonium-ion batteries as it reflects the transport kinetics during charge and discharge of the battery. Unfortunately, various cathodes reported to date have shown unsatisfactory rate performances, owing to the irreversible structural change in the electrode materials and intensive polarization of NH₄⁺ ions with slow charge transfer kinetics. However, the asprepared PPy shows excellent rate capability when subjected to harsh galvanostatic tests at a specific current ranging from 1 to 25 A g⁻¹ in a voltage window of -1 to 0.5 V, as presented in Fig. 3e. The PPy electrode shows the best performance for NH₄⁺ storage in the 25 m NH₄Ac electrolyte among all the electrolytes of different charge carriers or concentrations, demonstrating reversible capacities of 125.77, 106.50, 101.67, 80.88, 72.11, 60.13, 50.22, and 43.61 mA h g⁻¹ at specific currents of 1, 2, 5, 8, 10, 15, 20, and 25 A g^{-1} , respectively. It is noted that there is only \sim 19.16% capacity decay as the applied specific current is increased from 1 to 5 A g⁻¹. After being cycled at a high specific current of 25 A g^{-1} and back to 1 A g^{-1} , a capacity of 106.0 mA h

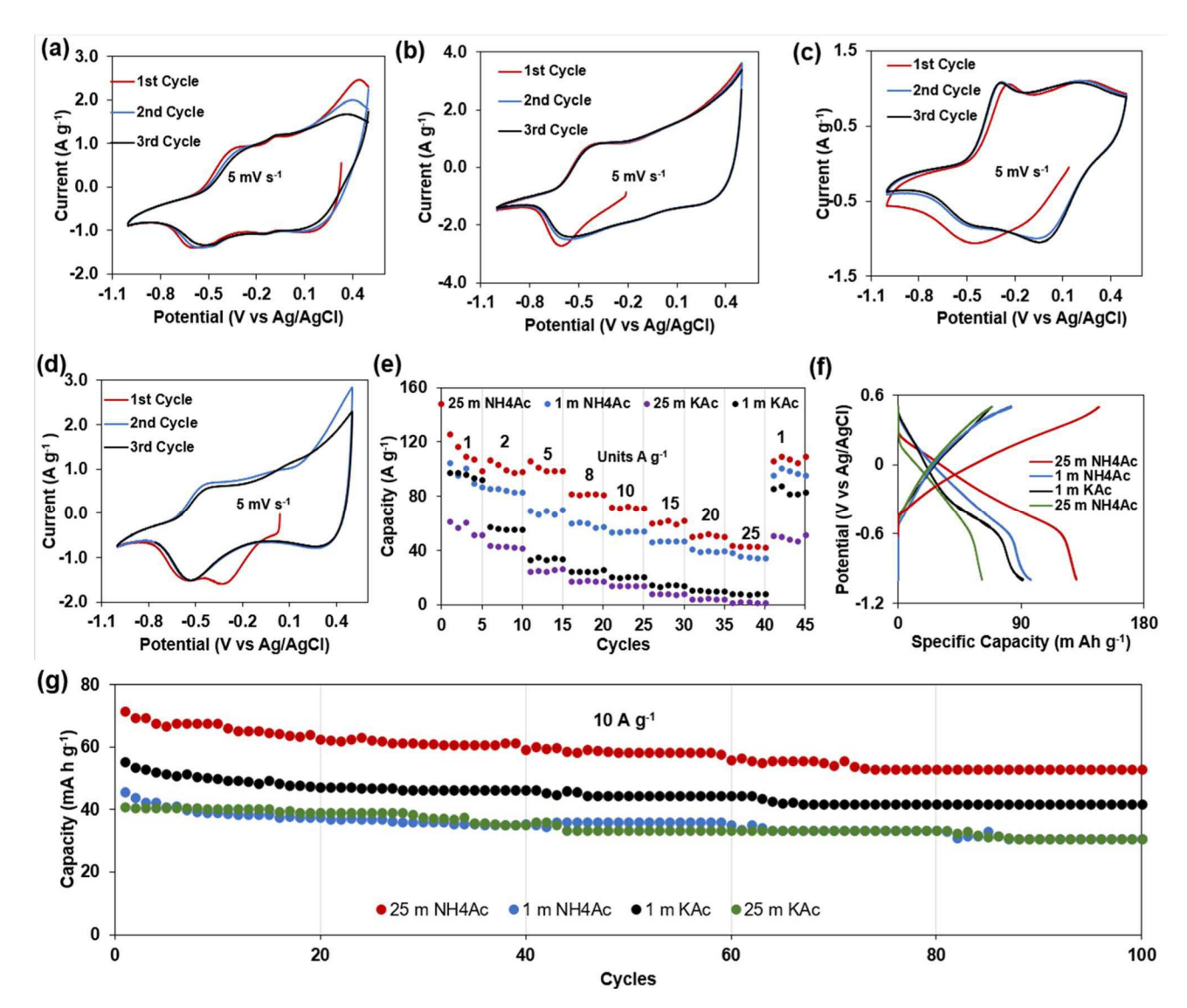


Fig. 3 The first three CV curves at a scan rate of 5 mV s⁻¹ of PPy cycled in (a) 25 m NH₄Ac, (b) 1 m NH₄Ac, (c) 25 m KAc, and (d) 1 m KAc. (e) Rate performances, (f) charge/discharge curves of initial cycles at 1 Å g^{-1} , and (g) cycling performances at 10 Å g^{-1} of PPy in 1 M and 25 m NH₄Ac and KAc electrolytes.

 g^{-1} is delivered, demonstrating the excellent structural integrity of the PPy electrode. Additionally, a moderate capacity of 43.61 mA h g⁻¹ and a discharge-charge time of 6.28 seconds, are delivered even at the highest specific current of 25 A g⁻¹, suggesting the ultrafast transport kinetics and impressive rate capability of the PPy electrode when cycled in the WiSE of ammonium ions. In the 1 m NH4Ac electrolyte, the PPy electrode exhibits discharge capacities of 104.44, 85.60, 66.94, 60.2, 53.19, 45.96, 38.89 and 35.97 mA h g^{-1} at specific currents of 1, 2, 5, 8, 10, 15, 20, and $25 \,\mathrm{A}\,\mathrm{g}^{-1}$, which are lower than those from the 25 m NH₄Ac electrolyte, due to the increased redox potential of PPy when tested in WiSE where more capacity could be realized at the same lower cutoff potential. The same phenomenon was observed for the titanic acid electrode in 25 m NH₄Ac.⁵³ On the other hand, PPy delivers a higher K⁺-storage capacity in the 1 m electrolyte than that in the 25 m KAc electrolyte. The former shows capacities of 97.22, 53.39, 33.33,

24.22, 20.22, 14.5, 10.61, and 7.88 mA h g^{-1} at specific currents of 1, 2, 5, 8, 10, 15, 20, and 25 A g^{-1} , respectively, while the latter exhibits capacities of 61.5, 42.83, 25.28, 17.10, 14.08, 7.85, 4.37, and 1.361 mA h g⁻¹, as shown in Fig. 3f. It is found that the K⁺storage performance of the PPy electrode is comparable with other host materials reported for K⁺ storage.^{57–59}

Fig. 3f exhibits the GCD curves of the PPy electrode in the different electrolytes, with the one for NH₄⁺ storage showing a smooth sloping profile and that for K+ storage containing a pronounced step or plateau. The coulombic efficiencies (CEs) calculated from Fig. 3f are 89.18 and 84.60% for PPy cycled in 25 and 1 m NH₄Ac, respectively, while CEs of PPy in 25 and 1 m KAc are 71% and 106%, respectively. The cycling performance of PPy in 25 and 1 m electrolytes of NH₄Ac and KAc are then examined at a high specific current of $10 \,\mathrm{Ag^{-1}}$, as displayed in Fig. 3g. The PPy cycled in 25 m NH₄Ac shows the highest initial capacity of 71.55 mA h g^{-1} and a capacity retention of 73.77% after 100

cycles, whereas PPy in 1 m NH_4Ac shows an initial capacity of 55.33 mA h g^{-1} and a capacity retention of 69.80% after 100 cycles. On the other hand, PPy cycled in 1 m KAc exhibits an initial capacity of 43.78 mA h g^{-1} and a capacity retention of 69.80% after 100 cycles, while PPy in 25 m KAc shows an initial capacity of 40.78 mA h g^{-1} and a capacity retention of 74.94% after 100 cycles. PPy demonstrates decent cycling stability for both NH_4^+ and K^+ storage in different electrolyte concentrations.

To elucidate the charge transfer process, electrochemical impedance spectroscopy (EIS) tests are then carried out in PPy when cycled in NH₄Ac and KAc electrolytes, as presented in Fig. S2.† The charge transfer resistances of PPy in 1 and 25 m NH₄Ac electrolytes are 8.31 and 9.28 Ω , respectively, while those in 1 and 25 m KAc electrolytes are 10.23 and 14.43 Ω , respectively. It can be seen that the charge transfer resistances of PPy in the 25 m electrolytes are higher than those in the 1 m electrolytes, possibly due to enhanced ion-ion interactions in WiSE. On another note, PPy in KAc electrolytes exhibits higher charge transfer resistances than in NH₄Ac at both concentrations, because K⁺ ions form rigid ionic bonds with water whereas NH₄ ions form weaker flexible hydrogen bonds with water which can break and form more easily during charge transport.60 This effect of strong coordination ability causing slower kinetics in KAc electrolyte is enhanced at higher concentrations, as more K⁺ ions form ionic bonds with water leading to higher interfacial resistance at the electrode/electrolyte interface. Hence, in addition to the electrolyte structure, the electrode/ electrolyte interfacial properties affect the charge transfer kinetics too.

To further study the kinetics in PPy for storage of K^+ and NH_4^+ ions, more CV tests are performed in 25 m electrolytes, as shown in Fig. 4. Fig. 4a and d present the CV profiles of the PPy electrode in 25 m NH_4 Ac and KAc, respectively, at sweep rates in a range of 1–10 mV s⁻¹. It is found that the CV profiles maintain similar shapes with the area getting larger with the increasing scan rate, indicating excellent electrochemical properties of PPy during the redox reactions with NH_4^+ and K^+ ions even in the 1 m electrolytes as presented in Fig. S3a and c.† The cathodic and anodic peaks appear to shift to low and high potentials at the increased scan rate, respectively, which can be attributed to the increase in diffusion resistance when the scan rate increases. The power law can be used to analyze the electrochemical kinetics, as described below:

$$i = av^b$$

where a and b are constants, v is the scan rate (in V s⁻¹), and i is the current (in A). b values represent the type of the electrochemical charge storage reaction and range between 0.5 and 1.0. If the b value is close to 0.5, the reaction is a diffusion-controlled process, while the b value being close to 1 indicates a capacitive process. Fig. 4b shows the b values to be 0.99 and 0.91, suggesting that the reaction is controlled by a capacitive process for NH₄⁺. The same can be said about K⁺ as revealed in

Fig. 4e with the b values being 1.04 and 1.07. When cycled in the 1 M electrolytes, the b values for $\mathrm{NH_4}^+$ are 0.90 and 0.93, showing that the reaction is capacitive controlled at even lower electrolyte concentrations (Fig. S3b†). It is different for PPY cycled in 1 M KAc electrolyte, because the b values are 0.72, 0.52 and 0.60 as revealed in Fig. S3d,† indicating that the reaction is mainly diffusion-controlled.

Furthermore, the equation $i = av^b$ can be separated into capacitive (k_1v) and diffusion $(k_2v^{1/2})$ factors to quantify their contributions:

$$i = k_1 v + k_2 v^{1/2}$$

With k_1 representing capacitive and k_2 diffusion contributions. Fig. 4c shows the capacitive contribution when PPy is cycled in 25 m NH₄Ac at 5 mV s⁻¹. As shown in Fig. 4g, 76.1% at 5 mV s⁻¹ is from capacitive contribution. Additionally, it can also be observed from Fig. 4g that as the scan rate increases, *i.e.*, 1, 3, 5, 8 and 10 mV s⁻¹, the capacitive process dominates the contribution towards the total capacity with contributions of 58.9, 71.2, 76.1, 80.2, and 81.9%, respectively. Similar to NH₄⁺, K⁺ also shows that at 5 mV s⁻¹ the capacity is dominated by capacitive controlled process as shown in Fig. 4h. Additionally, it can also be observed from Fig. 4h that as the scan rate increases, *i.e.*, 1, 3, 5, 8 and 10 mV s⁻¹, the capacitive process dominates the contribution towards the total capacity with contributions of 51, 64.5, 70.1, 74.7, and 76.8%, respectively.

To gain more insights into the storage mechanism of NH₄ ions in PPy, we conducted ex situ XPS spectroscopy on N 1s from the PPy electrode, since the electrochemical properties of PPy are dependent on the oxidation state of N. The study is focused on the PPy electrode cycled in 25 m NH₄Ac electrolyte, since it delivers the highest capacities among the battery cells using various electrolytes. Fig. 5 displays the N 1s XPS spectra of PPy at pristine, charge, and discharge states. As shown in Fig. 5a, the spectrum of pristine PPy reveals N 1s groups at 399.76, 398.07 and 401.11 eV, corresponding to N from -NH- (77.53%), -CN-(1.11%), and $-NH^+-$ (21.36%) (the value in the bracket is the atomic percentage). In the XPS spectrum of charged PPy after five cycles in Fig. 5b, the positions of N 1s peaks do not change, located at 399.66, 398.17, 401.53 and 404.68 eV, which represent non-protonated amine -NH- (63.58%), -NC- (6.14%), protonated amine $-NH^+$ – (29.73%) and -NO– (3.04%) nitrogen groups that are similar to the pristine state. Compared to the spectrum of discharged PPy in Fig. 5c, the atomic weight percentage of -NH⁺- increases from 29.73% in the charged state of PPy to 52.31% in its discharged state. As for the -NH- group, it decreases from 63.58% in charged PPy to 40.55% in discharged PPY, resulting from the oxidation of PPy by NH₄⁺ ions. As discharge continues and the potential on the electrode increases with the negative charges, more NH₄⁺ ions would be further attracted to the electrode and facilitate protonation of the -NH- group. The reverse process occurs during charging over a single potential range.

Due to the promising electrochemical performance of PPy in high-concentration NH_4Ac electrolyte, we then fabricate the first

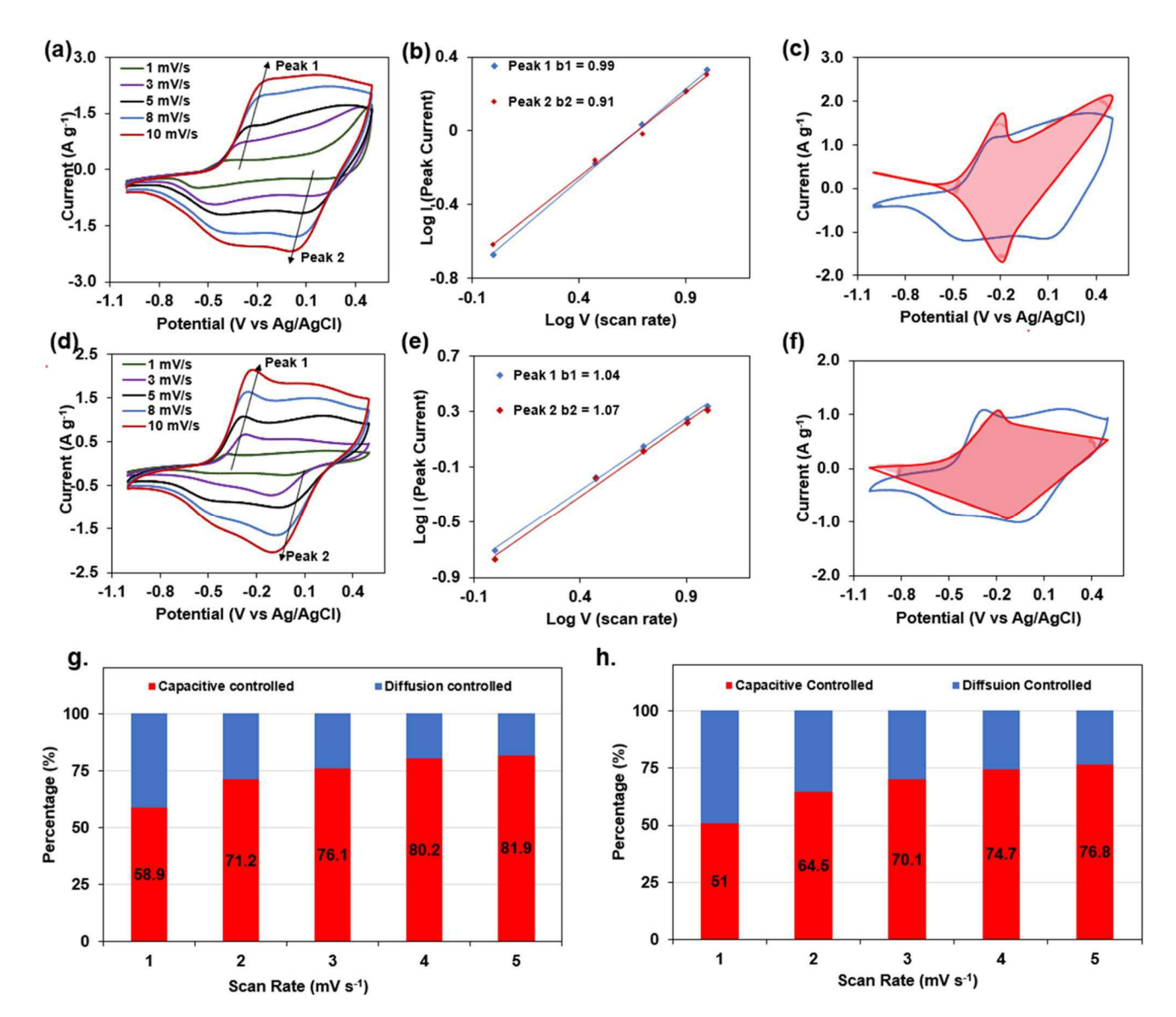


Fig. 4 Electrochemical tests of PPy in 25 m NH₄Ac electrolyte: (a) CV profiles at various scan rates, (b) $\log i$ (peak current) vs. $\log v$ (scan rate) based on the CV data in (a), and (c) CV showing the capacitive contribution at 5 mV s⁻¹. Electrochemical tests of PPY in 25 m KAc: (d) CV profiles at various scan rates, (e) log i (current) versus log v (scan rate) based on the CV data in (d), and (f) CV showing the capacitive contribution at 5 mV s $^{-1}$. The contribution ratio of the diffusion-controlled capacities and capacitive-controlled capacities for PPy in (g) 25 m NH_4 Ac electrolyte and (h) 25 m NH_4 Ac electrolyte a m KAc electrolyte.

all-organic metal-free battery and test it at 25 °C and 0 °C. Fig. S4† exhibits CV curves of PPy and PANI in the three-electrode cell using 25 m NH₄Ac electrolyte in the voltage range of 0.5 V to -1.0 V at 0 °C, to determine if any redox reaction occurs in these electrodes at such a low temperature. Fig. S4a† displays the first three CV curves of the PPy electrode, exhibiting cathodic peaks at 0.1 V and -0.2 V during the initial reduction scan. The oxidation peak at 0.05 V is observed too, which shows that PPy maintains its electrochemical activity even at 0 °C. On the other hand, the PANI electrode exhibits one major oxidation peak at 0.257 V and one reduction peak at -0.031 V. Both initial CV profiles of PPy and PANI display good repeatability, indicating good redox reversibility and structural stability at 0 °C. Encouraged by these results we assembled a full battery using

PANI as the anode and PPy as the cathode in the mass ratio of 1:1, as shown in Fig. 6. Aqueous NH₄Ac electrolytes of various concentrations have been studied and it was found that the 19 m NH₄Ac electrolyte has the lowest freezing point of -38 °C.⁶¹ Therefore, we prepare and compare full batteries using 19 m and 25 m NH₄Ac electrolytes.

Fig. 7a displays the first three CV curves of the PANI/PPy full cell with 19 m NH₄Ac electrolyte at 25 °C, revealing one pair of pronounced redox peaks at 0.085 V and 0.275 V, in the potential range of 0-1 V. No peak shift is observed when comparing these three CV profiles, demonstrating a reversible and stable redox reaction during charging and discharging of this full battery. To understand the kinetics of this full cell, we obtained its CV profiles at various scan rates ranging from 0.1 to 1 mV s⁻¹, as

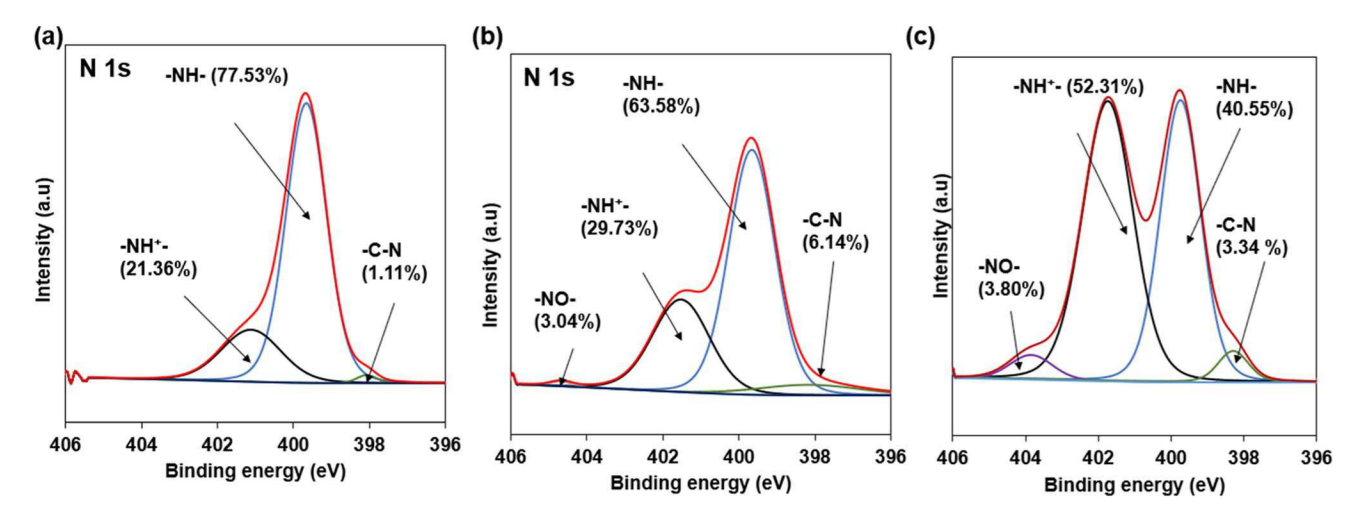


Fig. 5 Ex situ XPS N 1s spectra of PPy at (a) pristine, (b) charge, and (c) discharge states, when cycled in 25 m NH₄Ac.

shown in Fig. 7b. These CV curves at different scan rates show similar shapes, indicating the excellent structural integrity of the PANI and PPy electrodes. The power law based on the CV profiles in Fig. 7b is then applied to distinguish capacitive and diffusion currents. The *b* values for peaks 1 and 2 are found to be 0.91 and 0.80, respectively, as shown in Fig. 7c, suggesting that the electrochemical reactions in the full cell are controlled by both capacitive- and diffusion-controlled processes. It is expected that low temperature would affect the transport kinetics of charge carriers in electrolytes, thereby affecting conductivity and inevitably the performance of the full cell. Fig. 7d presents the first three CV curves of the full cell at 0 °C, presenting a pair

of redox peaks at 0.563/0.0088 V. It can be seen that the capacitive area of the CV curve at 25 °C is greater than that at 0 °C, because the conductivity and transport kinetics of the electrolyte are reduced at a lower temperature. The CV curves at various scan rates show great repeatability demonstrating that temperature is not affecting the redox peaks of either PPy or PANI as shown in Fig. 7e. The power law shows that the b values for peaks 1 and 2 are 0.81 and 0.74, showing that the process is dominated by the combination of capacitive and diffusion contributions, as seen in Fig. 7e.

To further explore the electrochemical performances of the full cells, the PANI/PPy full cell with 19 m or 25 m NH_4Ac

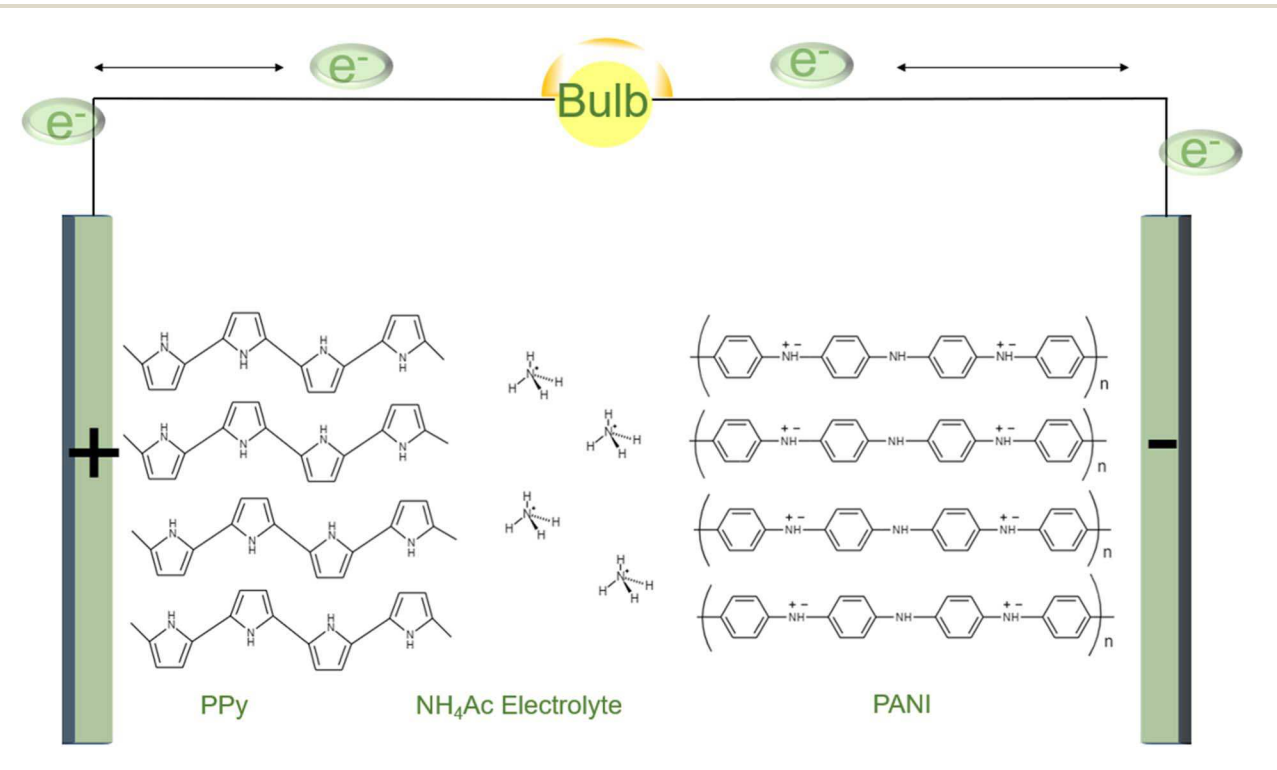


Fig. 6 Schematic of the metal-free ammonium-ion full battery based on PPY/PANI electrodes.

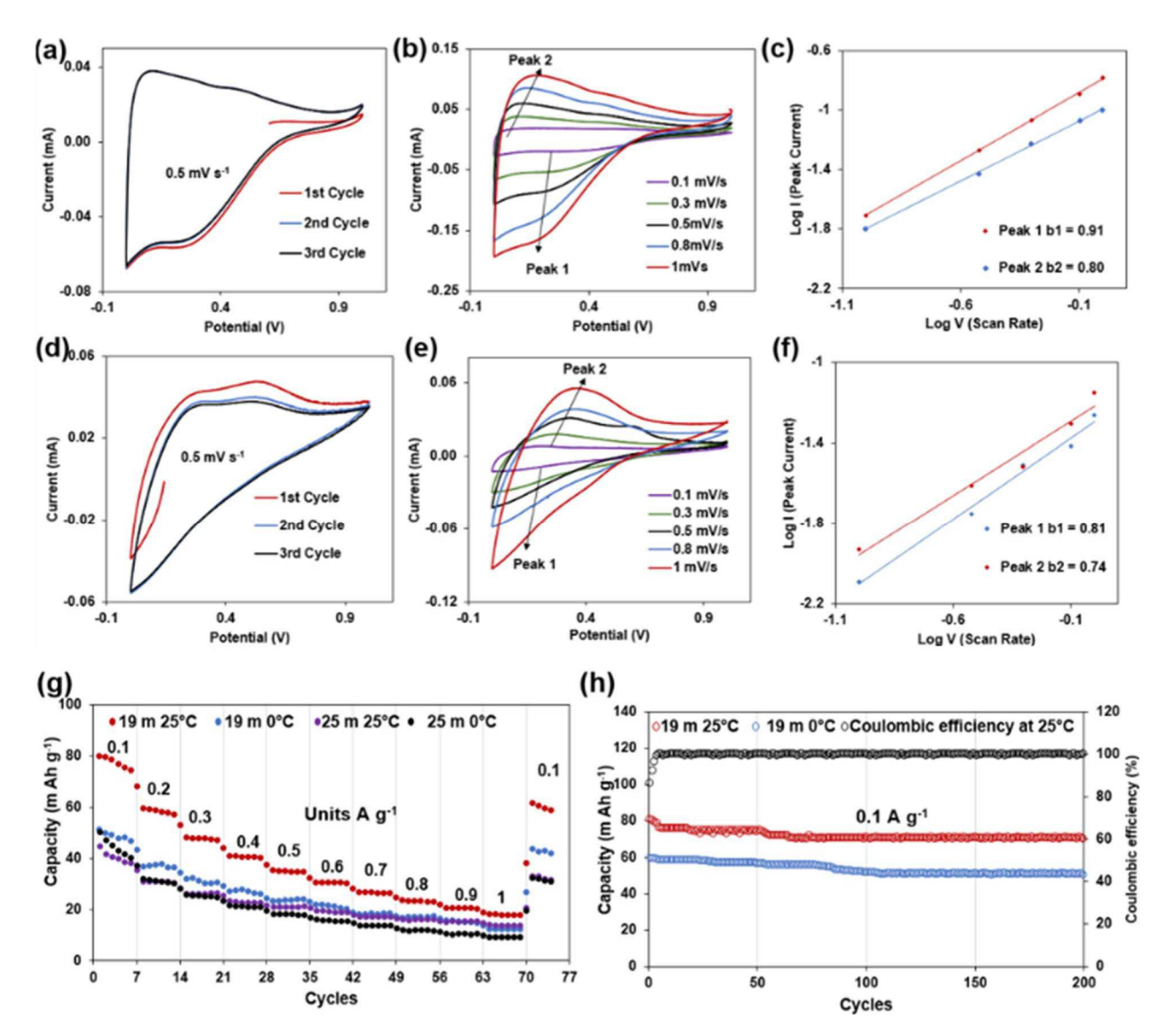


Fig. 7 Electrochemical performances of the full PANI/PPy AIB with 19 m NH₄Ac in the potential range of 0-1 V: (a) the first three CV curves at 0.5 mV s⁻¹ at 25 °C, (b) CV curves at various scan rates, (c) $\log i$ (current) *versus* $\log v$ (scan rate) at specific reduction/oxidation states based on the CV data in (b), (d) the first three CV curves at 0.5 mV s⁻¹ at 0 °C, (e) CV curves at various scan rates at 0 °C, and (f) $\log i$ (current) *versus* $\log v$ (scan rate) at specific reduction/oxidation states based on the CV data in (e). (g) Rate capability of PANI/PPy cells with 19 m and 25 m NH₄Ac electrolytes at 25 °C and 0 °C. (h) Cycling performances of the PANI/PPy cell with 19 m NH₄Ac electrolyte at 25 °C and 0 °C.

electrolyte is subjected to harsh galvanostatic evaluation from 0.1 to 1 A g^{-1} in a potential window of 0–1 V at 25 °C and 0 °C, as presented in Fig. 7g. The PANI/PPy full cell containing 19 m NH₄Ac exhibits reversible capacities of 78.405 and 49.083 mA h g^{-1} at 25 °C and 0 °C, respectively. Additionally, the cell based on the 25 m electrolyte delivers capacities of 45.184 and 40.633 mA h g^{-1} at 25 °C and 0 °C, respectively. The cell with 19 m electrolyte shows a capacity of 18.958 mA h g^{-1} at 1 A g^{-1} at 0 °C. Fig. 7h shows the cycling performance of the cell with 19 m electrolyte, presenting a retention capacity of 86.72% and 71.83% at a specific current of 0.1 A g^{-1} at 25 °C and 0 °C. For comparison purposes, a PANI/PPy full cell is assembled using 19 m KAc electrolyte, which delivers a very inferior capacity of 17.951 mA h g^{-1} at 0.1 A g^{-1} at 25 °C, as displayed in Fig. S5.† Fig. S6† exhibits the GCD curves of the full PANI/PPy cell at 25 °C.

C and 0 °C using 25 m and 19 m NH₄Ac electrolytes. The coulombic efficiencies (CEs) calculated from Fig. S6† are 120% and 115% for 19 m NH₄Ac electrolyte, as well as 113% and 108% for 25 m NH₄Ac electrolyte at 25 °C and 0 °C, respectively. The CEs are greater than 100%, which can be attributed to different storage capacities of PPy and PANI for NH₄⁺ ions. The NH₄⁺ ion is a more promising charge carrier for the PANI/PPy full battery and is the focus of this work. Fig. S7† exhibits the EIS spectra of the PANI/PPy full cell with 19 m NH₄Ac electrolyte at 0 °C and 25 °C, showing that the charge transfer resistance at 0 °C is 280 Ω and that at 25 °C is 88 Ω , confirming that the kinetics is slower at lower temperatures, thereby exhibiting a smaller capacity when temperature decreases. During the discharge process, NH₄⁺ ions will be stored in PPy through the mechanism described above; then NH₄⁺ ions move back into the electrolyte

during the charge process and will be stored in PANI via the mechanism reported by our group previously. ^{41,42} It can be seen that the capacity of our non-metal full battery is comparable to that delivered by an all-organic ammonium dual-ion battery composed of a graphite cathode and poly(1,5-naphthalenediamine) anode coupled with the electrolyte containing NH₄PF₆ dissolved in hybrid organic solvents reported recently, ⁶² however, the electrode and electrolyte materials in our work are more cost-effective. Yan *et al.* recently reported an ammonium-ion battery using a Prussian blue cathode and WiSE with preliminary results showing that the electrolyte can work over an extended temperature range of -40 to 80 °C, but the battery is not tested for cycling performance at low temperatures. ⁶³ Therefore, the PPy/PANI-based full battery in this work is the first one demonstrating low-temperature applications among AIBs and metal-free batteries.

Conclusion

In this work, we have developed the first all-organic metal-free battery that can operate at low temperatures, by using a PPY cathode and PANI anode as well as NH4Ac WiSE. First, PPY is systematically studied as a host material for both NH₄⁺ and K⁺ storage in electrolytes with 25 M and 1 M concentrations. It is found that PPY delivers an impressive capacity of 125 mA h ${
m g}^{-1}$ at a specific current of 1 Ag^{-1} and maintains 43.61 mA h g^{-1} at 25 A g⁻¹, when cycled in 25 M NH₄Ac electrolyte, much higher than 40.78 mA h $\rm g^{-1}$ at 1 A $\rm g^{-1}$ for $\rm K^+$ storage when it is cycled in 25 M KAc electrolyte. The PPy cathode is then coupled with the PANI anode together with 19 M NH_{4CH_{3COO}} electrolyte, to form a metal-free full cell that exhibits a high capacity of 78.405 mA h g^{-1} at 0.1 A g^{-1} at 25 °C and a capacity of 49.083 mA h g^{-1} at 0 ° C. Additionally, the physiochemical properties of NH₄⁺-based WiSEs are examined by Raman and nuclear magnetic resonance (NMR) spectroscopies, to explore their electrochemical behaviors and the fundamental effect of salt concentration on the electrolyte characteristics. This work presents new opportunities for the fabrication of all-organic batteries with lower cost, better safety and sustainability. Such a battery also opens the door to future realization of metal-free electronics that would generate long-term benefits to the environment.

Conflicts of interest

The authors declare no conflict of interests.

Acknowledgements

The authors acknowledge the Economic Development Assistantship, the LIFT2 fund from LSU, and REA (Research Enhancement Awards) grant from LaSPACE, for financial support. We also thank the LSU Shared Instrumentation Facilities (SIF) for assistance with materials characterization.

References

- 1 F. Sun, M. Osenberg, K. Dong, D. Zhou, A. Hilger, C. J. Jafta, S. Risse, Y. Lu, H. Markötter and I. Manke, *ACS Energy Lett.*, 2018, 3(2), 356–365.
- 2 C.-C. Li and Y.-W. Wang, *J. Power Sources*, 2013, 227, 204–210.
- 3 W.-J. Zhang, J. Power Sources, 2011, 196(6), 2962-2970.
- 4 G. Vitins and K. West, J. Electrochem. Soc., 1997, 144(8), 2587.
- 5 J. B. Goodenough and Y. Kim, *Chem. Mater.*, 2010, 22(3), 587–603.
- 6 M. S. Whittingham, Chem. Rev., 2004, 104(10), 4271-4302.
- 7 K. Turcheniuk, D. Bondarev, V. Singhal and G. Yushin, *Nature*, 2018, 559, 467–470.
- 8 J. Peng, Z. Wang, Q. Liu, J. Wang, S. Chou, H. Liu and S. Dou, *Adv. Mater.*, 2022, 34(15), 2108384.
- 9 F. Yuan, Z. Li, D. Zhang, Q. Wang, H. Wang, H. Sun, Q. Yu, W. Wang and B. Wang, Adv. Sci., 2022, 2200683.
- 10 T. Han, Y. Wang, H. Bai, H. Zhang and J. Liu, *Chem. Commun.*, 2022, **58**, 7172–7175.
- 11 Y. Lv, Y. Xiao, L. Ma, C. Zhi and S. Chen, *Adv. Mater.*, 2022, 34(4), 2106409.
- 12 A. Michail, B. Silván and N. Tapia-Ruiz, *Curr. Opin. Electrochem.*, 2022, 31, 100817.
- 13 Y. Wang and S. F. Kuchena, *ACS Omega*, 2022, 7(38), 33732–33748.
- 14 C. D. Wessells, M. T. McDowell, S. V. Peddada, M. Pasta, R. A. Huggins and Y. Cui, *ACS Nano*, 2012, **6**(2), 1688–1694.
- 15 X. Wu, Y. Qi, J. J. Hong, Z. Li, A. S. Hernandez and X. Ji, *Angew. Chem., Int. Ed.*, 2017, **56**(42), 13026–13030.
- 16 H. Zhang, Y. Tian, W. Wang, Z. Jian and W. Chen, *Angew. Chem.*, 2022, **61**(27), 1-5.
- 17 X. Wu, Y. Xu, H. Jiang, Z. Wei, J. J. Hong, A. S. Hernandez, F. Du and X. Ji, ACS Appl. Energy Mater., 2018, 1(7), 3077– 3083.
- 18 M. Xia, X. Zhang, H. Yu, Z. Yang, S. Chen, L. Zhang, M. Shui, Y. Xie and J. Shu, *Chem. Eng. J.*, 2021, **421**, 127759.
- 19 C. D. Wessells, S. V. Peddada, M. T. McDowell, R. A. Huggins and Yi Cui, *J. Electrochem. Soc.*, 2011, **159**, A98.
- 20 J. Xing, X. Fu, S. Guan, Y. Zhang, M. Lei and Z. Peng, *Appl. Surf. Sci.*, 2021, 543, 148843.
- 21 C. Li, W. Yan, S. Liang, P. Wang, J. Wang, L. Fu, Y. Zhu, Y. Chen, Y. Wu and W. Huang, *Nanoscale Horiz.*, 2019, 4(4), 991–998.
- 22 C. Li, D. Zhang, F. Ma, T. Ma, J. Wang, Y. Chen, Y. Zhu, L. Fu, Y. Wu and W. Huang, *ChemSusChem*, 2019, 12(16), 3732–3736.
- 23 X. Wu, Y. Qi, J. J. Hong, Z. Li, A. S. Hernandez and X. Ji, *Angew. Chem., Int. Ed.*, 2017, **56**(42), 13026–13030.
- 24 G. Liang, Y. Wang, Z. Huang, F. Mo, X. Li, Y. Qi, D. Wang, H. Li, S. Chen and C. Zhi, *Adv. Mater.*, 2020, 32(14), 1907802.
- 25 S. Dong, W. Shin, H. Jiang, X. Wu, Z. Li, J. Holoubek, W. F. Stickle, et al., Chem, 2019, 5(6), 1537–1551.
- 26 W. Xu, L. Zhang, K. Zhao, X. Sun and Q. Wu, *Electrochim. Acta*, 2020, 360, 137008.

- 27 S. Kuchena and Y. Wang, *Chem.-Eur. J.*, 2021, 27, 15450–15459.
- 28 Y. Song, Q. Pan, H. Lv, D. Yang, Z. Qin, M. -Y. Zhang, X. Sun and X. -X. Liu, *Angew. Chem., Int. Ed.*, 2021, **60**(11), 5718–5722.
- 29 L. Suo, O. Borodin, T. Gao, M. Olguin, J. Ho, X. L. Fan, C. Luo, C. S. Wang and K. Xu, *Science*, 2015, 350, 938–943.
- 30 J. J. Holoubek, H. Jiang, D. Leonard, Y. Qi, G. C. Bustamante and Ji. Xiulei, *Chem. Commun.*, 2018, **54**(70), 9805–9808.
- 31 C. P. Grey and J. M. Tarascon, *Nat. Mater.*, 2017, **16**(1), 45–56.
- 32 P. Poizot, J. Gaubicher, S. Renault, L. Dubois, Y. Liang and Y. Yao, *Chem. Rev.*, 2020, **120**(14), 6490–6557.
- 33 K. Deuchert and S. Hünig, *Angew. Chem., Int. Ed. Engl.*, 1978, **17**(12), 875–886.
- 34 B. Esser, F. Dolhem, M. Becuwe, P. Poizot, A. Vlad and D. Brandell, *J. Power Sources*, 2021, **482**, 228814.
- 35 H. Kye, Y. Kang, D. Jang, J. E. Kwon and B.-G. Kim, *Adv. Energy Sustain. Res.*, 2022, 2200030.
- 36 Z. Zhao, Y. Lei, L. Shi, Z. Tian, M. Hedhili, Y. Khan and H. N. Alshareef, *Angew. Chem., Int. Ed.*, 2022, **61**(51), 1–7.
- 37 J. Han, Z. Chen and J. Xu, Mater. Lett., 2021, 304, 130629.
- 38 J. Huang, Z. Wang, M. Hou, X. Dong, Y. Liu, Y. Wang and Y. Xia, *Nat. Commun.*, 2018, **9**(1), 1–8.
- 39 R. Li, F. Xing, T. Li, H. Zhang, J. Yan, Q. Zheng and X. Li, *Energy Storage Mater.*, 2021, **38**, 590–598.
- 40 J.-W. Xu, Q.-L. Gao, Y.-M. Xia, X.-S. Lin, W.-L. Liu, M.-M. Ren, F.-G. Kong, S.-J. Wang and C. Lin, *J. Colloid Interface Sci.*, 2021, 598, 419–429.
- 41 S. F. Kuchena and Y. Wang, *ACS Appl. Energy Mater.*, 2020, 3(12), 11690–11698.
- 42 S. F. Kuchena and Y. Wang, *Electrochim. Acta*, 2022, 425, 140751.
- 43 S. Dong, W. Shin, H. Jiang, X. Wu, Z. Li, J. Holoubek, W. F. Stickle, et al., Chem, 2019, 5(6), 1537–1551.
- 44 A. Kausaite-Minkstimiene, V. Mazeiko, A. Ramanaviciene and A. Ramanavicius, *Colloids Surf.*, A, 2015, 483, 224–231.
- 45 R. Ansari, E-J. Chem., 2006, 3(4), 186-201.
- 46 B. Zhang, Y. Xu, Y. Zheng, L. Dai, M. Zhang, Y. Jin, Y. Chen,X. Chen and J. Zhou, *Nanoscale Res. Lett.*, 2011, 6(1), 1–9.

- 47 Y. Wang and S. F. Kuchena, *ACS Omega*, 2022, 7(38), 33732–33748.
- 48 C. MA, S. G. Pawar, P. R. Godse, S. Sen and V. B. Patil, *Soft Nanosci. Lett.*, 2011, 1(1), 6–10.
- 49 Y. Yamada, K. Usui, K. Sodeyama, S. Ko, Y. Tateyama and A. Yamada, *Nat. Energy*, 2016, **1**(10), 1–9.
- 50 L. Coustan, G. Shul and D. Belanger, *Electrochem. Commun.*, 2017, 77, 89–92.
- 51 M. Amiri and D. Bélanger, *ChemSusChem*, 2021, **14**(12), 2487–2500.
- 52 M. H. Lee, S. J. Kim, D. Chang, J. Kim, S. Moon, K. Oh, K.-Y. Park, et al., Mater. Today, 2019, 29, 26–36.
- 53 T. Liu, L. Tang, H. Luo, S. Cheng and M. Liu, *Chem. Commun.*, 2019, 55(85), 12817–12820.
- 54 N. Dubouis, P. Lemaire, B. Mirvaux, E. Salager, M. Deschamps and A. Grimaud, *Energy Environ. Sci.*, 2018, 11(12), 3491–3499.
- 55 J. J. Holoubek, H. Jiang, D. Leonard, Y. Qi, G. C. Bustamante and J. Xiulei, *Chem. Commun.*, 2018, 54(70), 9805–9808.
- 56 Z. Tian, V. S. Kale, Y. Wang, S. Kandambeth, J. Czaban-Jozwiak, O. Shekhah, E. Mohamed and H. N. Alshareef, *J. Am. Chem. Soc.*, 2021, 143(45), 19178–19186.
- 57 Q. Zhang, Z. Wang, S. Zhang, T. Zhou, J. Mao and Z. Guo, *Electrochem. Energy Rev.*, 2018, **1**(4), 625–658.
- 58 M. Sha, L. Liu, H. Zhao and Y. Lei, Review on recent advances of cathode materials for potassium-ion batteries, *Energy Environ. Mater.*, 2020, 3(1), 56–66.
- 59 Z. Wu, J. Zou, S. Chen, X. Niu, J. Liu and L. Wang, *J. Power Sources*, 2021, **484**, 229307.
- 60 Z. Tian, V. S. Kale, Y. Wang, S. Kandambeth, J. Czaban-Jozwiak, O. Shekhah, E. Mohamed and H. N. Alshareef, *J. Am. Chem. Soc.*, 2021, 143(45), 19178–19186.
- 61 L. Yan, Y.-E. Qi, X. Dong, Y. Wang and Y. Xia, *eScience*, 2021, 1(2), 212–218.
- 62 Z. Zhao, Y. Lei, L. Shi, Z. Tian, M. Hedhili, Y. Khan and H. N. Alshareef, *Angew. Chem., Int. Ed.*, 2022, **61**(51), 1–7.
- 63 L. Yan, Y.-E. Qi, X. Dong, Y. Wang and Y. Xia, *eScience*, 2021, 1(2), 212–218.